Catalysis Science & Technology

PAPER

View Article Online
View Journal | View Issue

Cite this: *Catal. Sci. Technol.*, 2017, 7, 5585

Further insight into the electrocatalytic water oxidation by macrocyclic nickel(II) complexes: the influence of steric effect on catalytic activity†

Jia-Wei Wang, [a] Cheng Hou,[a] Hai-Hua Huang, [a] Wen-Ju Liu,[a] Zhuo-Feng Ke *[a] and Tong-Bu Lu *[ab]

Received 28th July 2017,
Accepted 28th September 2017

DOI: 10.1039/c7cy01527e

rsc.li/catalysis

The development of efficient, robust and economical water oxidation catalysts (WOCs) remains a key challenge for water splitting. Herein, three macrocyclic nickel(II) complexes with four, six and eight methyl groups in the ligands have been utilized as homogeneous electrocatalysts for water oxidation in aqueous phosphate buffer at pH 7.0, in which the catalyst with eight methyl groups exhibits the highest catalytic activity, with a large current density of 1.0 mA cm^{-2} at 1.55 V *vs.* NHE (750 mV overpotential) in long-term electrolysis. The results of electrochemistry, UV-vis spectroelectrochemistry and DFT calculations suggest that the axially oriented methyl groups in the macrocyclic ligands with eight and six methyl groups can impose a steric effect on the axial position of the Ni^{III} center, which not only results in higher $Ni^{III/II}$ oxidation potentials but also suppresses the axial coordination of phosphate anions with the Ni^{III} center to achieve better catalytic performance. Such a steric effect in homogeneous WOCs has not been reported so far.

Introduction

Water oxidation has been considered as the bottleneck half-reaction of water splitting, a promising way to produce large-scale hydrogen as renewable and clean energy.[1] In this context, the development of efficient, robust and economical water oxidation catalysts (WOCs) is of growing interest. Although the performances of these homogeneous WOCs are not comparable to those of heterogeneous WOCs,[2] their homogeneous nature enables more in-depth mechanistic investigations. Moreover, homogeneous WOCs have shown additional appealing features, such as tunable redox properties and ease of optimization *via* synthetic means.[3] Up to now, homogeneous WOCs based on Ru (ref. 4) and Ir (ref. 5) have been highly efficient, while their applications are limited by their scarcity. Hence, a number of homogeneous WOCs based on earth-abundant metals, such as V,[6] Mn,[7] Fe,[8] Ni,[9] Co (ref. 10) and Cu,[11] have been reported. However, many of these were used in highly basic or acidic solutions;[6a,8b,9d,11a,b,12] only a few WOCs were used at neutral pH.[9a–c,11d] Moreover, some reported WOCs are vulnerable to decomposition and/or deactivation under highly oxidizing conditions.[7c,8a,11a,b,12d,13] Therefore, the design and synthesis of cheap and stable WOCs operating at neutral pH still remains a challenge.

Recently, homogeneous WOCs based on nickel complexes continue to attract attention owing to their rich redox properties and the highly oxidizing power of Ni^{III} and Ni^{IV}

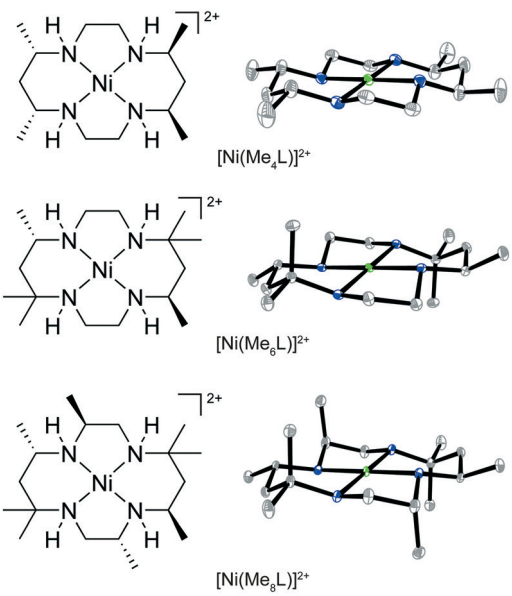

Fig. 1 The schematic (left) and crystallographic (right) structures of the macrocyclic nickel(II) complexes. Hydrogen and counter anions are omitted for clarity. Thermal ellipsoids are drawn at the 30% level.

[a] *MOE Key Laboratory of Bioinorganic and Synthetic Chemistry, School of Chemistry, Sun Yat-Sen University, Guangzhou 510275, China. E-mail: kezhf3@mail.sysu.edu.cn, lutongbu@mail.sysu.edu.cn*
[b] *Institute for New Energy Materials & Low Carbon Technologies, School of Materials Science & Engineering, Tianjin University of Technology, Tianjin 300384, China*

† Electronic supplementary information (ESI) available: Experimental and computational details and additional data. See DOI: 10.1039/c7cy01527e

species.[9b,d] Following our report on the first nickel homogeneous WOC based on a nickel(II) macrocyclic complex, $[Ni(Me_6L)](ClO_4)_2$ (Me_6L = (7*R*,14*S*)-5,5,7,12,12,14-hexamethyl-1,4,8,11-tetraazacyclo-tetradecane, Fig. 1),[9a] a handful of nickel(II) complexes have been documented as homogeneous WOCs, including a nickel porphyrin,[9b] nickel amine–pyridine complexes,[9c] a nickel penta–pyridine complex[9d] and polynuclear nickel-centered polyoxometalates.[9e,14] However, these subsequent nickel WOCs generally exhibit relatively low catalytic efficiency[9b,c,e] or require a high overpotential.[9d] In contrast, the relatively large current density achieved at neutral pH, remarkable robustness and easy synthesis of $[Ni(Me_6L)](ClO_4)_2$ stand out among the reported nickel homogeneous WOCs. Thus, we were motivated to further optimize the catalytic performance of this WOC, which can be achieved by rational modification of the structure of the macrocyclic ligand.

To this end, we have tried to vary the amount of methyl groups in the structure of the macrocyclic ligand to observe the effect on the catalytic performance, as methyl groups may induce a steric effect on the active intermediate formed during water oxidation.[15] Notably, investigations of steric effects on the catalytic performance of homogeneous WOCs are rare.[16] In the present work, two additional macrocyclic nickel(II) complexes, namely, $[Ni(Me_4L)](ClO_4)_2$ and $[Ni(Me_8L)](ClO_4)_2$, were synthesized (Fig. 1; Me_4L = (5*S*,7*R*,12*R*,14*S*)-5,7,12,14-tetramethyl-1,4,8,11-tetraazacyclo-tetradecane, Me_8L = (2*S*,7*R*,9*R*,14*S*)-2,5,5,7,9,12,12,14-octamethyl-1,4,8,11-tetraazacyclotetradecane), and their electrocatalytic performance for water oxidation was investigated. The results reveal that $[Ni(Me_8L)](ClO_4)_2$ displays higher electrocatalytic activity than $[Ni(Me_6L)](ClO_4)_2$, while $[Ni(Me_4L)](ClO_4)_2$ shows lower electrocatalytic activity than $[Ni(Me_6L)](ClO_4)_2$. The different catalytic abilities may originate from the steric repulsion between the axial methyl groups and the phosphate anions that are axially coordinated to the *in situ* formed Ni^{III} species during water oxidation.

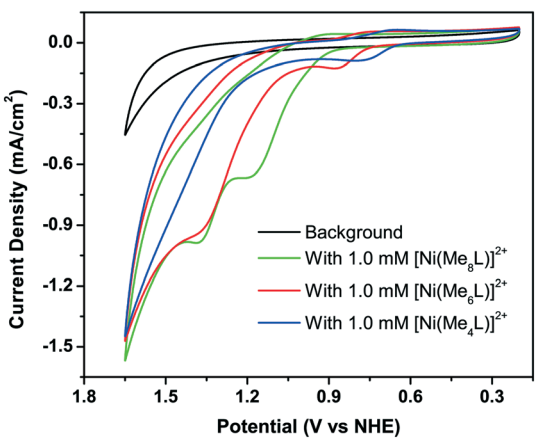

Fig. 2 CVs of 1.0 mM $[Ni(Me_4L)](ClO_4)_2$ (blue), $[Ni(Me_6L)](ClO_4)_2$ (red) and $[Ni(Me_8L)](ClO_4)_2$ (green) in 0.10 M NaPi buffer at pH 7.0; scan rate = 100 mV s^{-1}. The background (black) is shown for comparison.

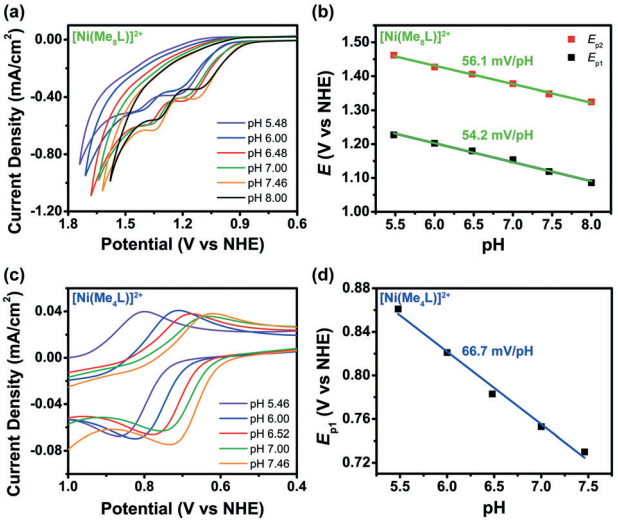

Fig. 3 (a) CVs of 1.0 mM $[Ni(Me_8L)](ClO_4)_2$ in 0.10 M NaPi buffer at varied pH (scan rate = 25 mV s^{-1}) and (b) plot of the two wave positions *versus* pH values. (c) CVs of 1.0 mM $[Ni(Me_4L)](ClO_4)_2$ in 0.10 M NaPi buffer at varied pH (scan rate = 25 mV s^{-1}) and (d) corresponding linear fittings for the wave positions *versus* pH values.

Experimental section

Materials

All of the chemicals are commercially available and used without further purification. All the solutions were prepared with Milli-Q ultrapure water (>18 MΩ) unless otherwise stated. Indium tin oxide (ITO) glass (6–7 ohms) was purchased from Kaivo Electronic Components Co., Ltd. The Pt foil electrode, AgCl/Ag reference electrode, glassy carbon (GC) electrode and spectroelectrochemistry cell (UV-4000) were purchased from Gauss Union Technology Co. Ltd.

Characterization

Elemental analysis (C, H, N) results were collected using a Vario EL elemental analyzer. UV-vis spectra were obtained using a Shimadzu UV-3600 spectrophotometer. Scanning electron microscopy (SEM) and energy dispersive X-ray spectroscopy (EDX) results were obtained using a Quanta 400 field emission SEM. The single-crystal X-ray diffraction data were collected using an Agilent Technologies Gemini A Ultra system under Cu/Kα radiation (λ = 1.54178 Å) at 150 K. Powder X-ray diffraction (PXRD) data were recorded on a Bruker D8 Advance diffractometer (Cu/Kα) at room temperature. Electrochemical measurements were carried out using a CHI 760E workstation. Unless otherwise stated, all the electrochemical experiments were conducted at 24–25 °C with all potentials footnoted as *versus* a normal hydrogen electrode (*vs.* NHE). A three-electrode set-up, including a Pt foil (1.0 cm^2) as the counter electrode, an Ag/AgCl electrode as the reference electrode (saturated aqueous KCl as the inner electrolyte; +0.197 V *vs.* NHE), and a 3 mm GC electrode as the working electrode, was used for cyclic voltammetry measurements. Oxygen detection was conducted *via* a gas

Table 1 The calculated and measured redox potentials of the three nickel(II) complexes and the O–Ni–N_x (x = 1 or 2) angles in the three optimized nickel(III) structures in Scheme 2

Complexes	$[Ni(Me_4L)](ClO_4)_2$	$[Ni(Me_6L)](ClO_4)_2$	$[Ni(Me_8L)](ClO_4)_2$
Calculated $E(Ni^{III/II})$ (V)	0.81	0.86	0.99
Measured $E(Ni^{III/II})$ (V)	0.77	0.87	1.15
Calculated $E(Ni^{IV/III})$ (V)	1.44	1.44	1.40
Measured $E(Ni^{IV/III})$ (V)	1.40	1.40	1.38
O–Ni–N_1 (°)	99.55	103.60	103.32
O–Ni–N_2 (°)	98.20	99.63	104.81

chromatograph (Agilent 7820A-GC, 5 Å molecular sieve column, thermal conductivity detector).

Controlled potential electrolysis and oxygen detection

Controlled potential electrolysis (CPE) experiments were carried out in a three-compartment, three-electrode cell without iR correction. A Pt foil was used as the counter electrode and ITO glass (1.5 cm^2 immersed in electrolyte) was used as the working electrode, both of which were facing each other. The counter electrode compartment (containing 3.5 mL electrolyte) was separated from the working electrode compartment (containing 3.5 mL electrolyte) by a porosity frit. An Ag/AgCl reference electrode was placed in the third compartment and attached to the working electrode compartment with a Luggin capillary. During CPE, any movement or shaking of the cell would interfere with the current traces. For the detection of oxygen, the three compartments were firmly sealed up and purged with argon for 30 min. The gas products from the working electrode compartment were analyzed by gas chromatography. The chromatographic response for O_2 was normalized to residual O_2/N_2 from ambient air when calculating the corresponding Faradaic efficiency.

Caution! *Perchlorate salts of metal complexes are potentially explosive and should be used with care.*

Synthesis of $[Ni(Me_6L)](ClO_4)_2$

The Me_6L ligand[17] and its nickel complex[18] were synthesized according to literature methods. Anal. calcd for $C_{16}H_{36}Cl_2N_4NiO_8$ (%): C 35.45, H 6.69, N 10.34; found: C 35.59, H 6.83, N 10.50.

Synthesis of $[Ni(Me_8L)](ClO_4)_2$

The Me_8L ligand and its nickel complex were synthesized according to a literature method.[19] Anal. calcd for $C_{18}H_{40}Cl_2N_4NiO_8$ (%): C 37.92, H 7.07, N 9.83; found: C 38.05, H 7.13, N 9.92.

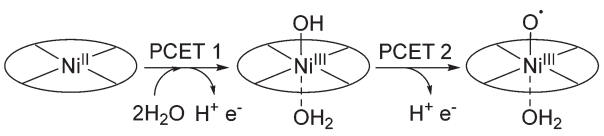

Scheme 1 Two steps of PCETs during water oxidation catalyzed by the macrocyclic nickel(II) complexes.

Synthesis of $[Ni(Me_4L)](ClO_4)_2$

The crude product was prepared by $NaBH_4$ reduction of the unsaturated nickel–diene complex,[20] which was further purified by two recrystallizations from its 6 M $NaClO_4$ aqueous solution.[21] Anal. calcd for $C_{14}H_{32}Cl_2N_4NiO_8$ (%): C 32.71, H 6.27, N 10.90; found: C 32.52, H 6.25, N 10.84.

Recovery of $[Ni(Me_4L)](ClO_4)_2$ and $[Ni(Me_8L)](ClO_4)_2$ from the electrolytes

The above two nickel complexes in the electrolytes after CPE could be recovered as reddish orange crystals by slow evaporation of the electrolytes in a desiccator for 20 d. For $[Ni(Me_4L)](ClO_4)_2$, 1.7 mg (83%) crystals could be recovered from ~4 mL used electrolyte. For $[Ni(Me_8L)](ClO_4)_2$, 2.1 mg (92%) crystals could be recovered from ~4 mL used electrolyte.

Detection of peroxide intermediates in electrolyte[22]

Ampliflu red (AR) and horseradish peroxidase (HRP, >160 units per mg) were dissolved in dimethyl sulphoxide and 0.1 M neutral NaPi buffer, respectively, both in a concentration of 0.4 mg mL^{-1}. The electrolyte for the detection of peroxide intermediates was obtained either from continuous scanning for 100 cycles of cyclic voltammetry within the 0.5–1.6 V range or from a CPE experiment at 1.55 V with **1**. Then the horseradish peroxidase solution (1.0 mL) and Ampliflu red solution (1.0 mL) were instantly added into the resulting electrolyte (0.4 mL).

DFT calculation

All the calculations were performed *via* the Gaussian 09 program.[23] All the structures were fully optimized at the B3LYP[24]/BSI level (BSI designated the basis set combination

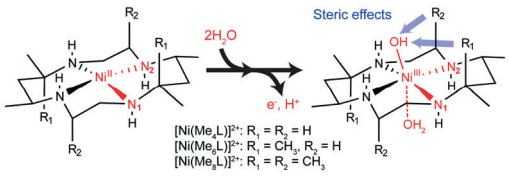

Scheme 2 The steric effect between the axially coordinated ligand and the axially oriented methyl groups during the $Ni^{III/II}$-involved PCET process.

Table 2 The measured current densities, TONs and Faradaic efficiencies of the three nickel WOCs during 5 h of CPE

Complexes	$[Ni(Me_4L)](ClO_4)_2$	$[Ni(Me_6L)](ClO_4)_2$	$[Ni(Me_8L)](ClO_4)_2$
Current density (mA cm^{-2})	0.25 ± 0.02	0.90 ± 0.03	1.05 ± 0.05
TON	3.6 ± 0.3	13.0 ± 0.5	15.2 ± 0.8
Faradaic efficiency (%)	94% ± 5%	97% ± 4%	93% ± 5%

of SDD[25] for the Ni atom and 6-31g (d,p) for non-metal atoms). Frequency analysis calculations were performed to characterize the structures as minima or transition states. IRC calculations were adopted to confirm the connection of the transition state and its two relevant minima. At B3LYP/BSI optimized geometries, the free energy results were further refined by calculating the single point energy at BLYP* (17% exact exchange)/BSII level (BSII designated SDD for the Ni atom and 6-311++g (d,p) for nonmetal atoms). The BLYP* method containing 17% HF exchange component was found to be appropriate for reproducing the experimental redox potential. The 3D optimized structure figures in this paper were drawn using the CYLview visualization program.[26]

Results and discussion

Investigations on the redox properties

Cyclic voltammetry was applied to investigate the redox properties of $[Ni(Me_8L)](ClO_4)_2$ and $[Ni(Me_4L)](ClO_4)_2$ in 0.10 M sodium phosphate (NaPi) buffer at pH 7.0, with the reported $[Ni(Me_6L)](ClO_4)_2$ as a contrast.[8a] $[Ni(Me_8L)](ClO_4)_2$ was studied first. As shown in Fig. 2 and S1,† an irreversible oxidation wave appeared at 1.15 V in the cyclic voltammogram (CV) of $[Ni(Me_8L)](ClO_4)_2$, attributable to one-electron oxidation of Ni^{II} to Ni^{III}. This oxidation wave is pH-dependent (Fig. 3a), with the anodic peak potentials *versus* pH decreasing by ~56 mV per pH unit (Fig. 3b), indicating that the $Ni^{III/II}$ oxidation undergoes a 1 e^-/1 H^+ proton-coupled electron transfer (PCET).[27] At a more positive potential, the CV of $[Ni(Me_8L)](ClO_4)_2$ featured an additional irreversible oxidation wave at 1.38 V, with a much higher current compared to the background. This observation suggests an electrocatalytic process, possibly water oxidation, and the products will be verified later by CPE. The currents at 1.38 V increased linearly with increasing concentrations of $[Ni(Me_8L)](ClO_4)_2$ (Fig. S2†), suggesting single-site catalysis. Additionally, the second oxidation wave of $[Ni(Me_8L)](ClO_4)_2$ also undergoes a 1 e^-/1 H^+ PCET, as determined by cyclic voltammetry at varying pH (Fig. 3b). As for $[Ni(Me_4L)](ClO_4)_2$, its CV features a quasi-reversible couple at 0.77 V, assignable to the $Ni^{III/II}$ couple (Fig. 2). This couple also undergoes a 1 e^-/1 H^+ PCET according to the pH-dependent CVs (Fig. 3c). Actually, an additional irreversible oxidation wave near 1.40 V was observed in the initial scans of the CV of $[Ni(Me_4L)](ClO_4)_2$, which is also indicative of an electrocatalytic process. This wave disappeared after several repeated scans (Fig. S3†), suggesting that the further oxidized species may be short-lived, and a similar phenomenon has also been observed in other molecular WOCs.[10b] Notably, upon the addition of H_2O_2 to 1.0 mM of each catalyst in 0.10 NaPi buffer at pH 7.0, the oxidation current of Ni^{II} to Ni^{III} increased relative to the background, and the catalytic current increased with increasing concentrations of H_2O_2 (Fig. S4†), demonstrating the Ni^{III} species can catalyze the oxidation of H_2O_2 to O_2.[9a]

Interestingly, as shown in Fig. 2, the $Ni^{III/II}$ oxidation peaks of the three nickel complexes exhibit a positive shift with increasing methyl groups (see Table 1). Meanwhile, an enhancement of the irreversibility of the $Ni^{III/II}$ couple could be observed, as demonstrated by the CVs of $[Ni(Me_6L)](ClO_4)_2$ and $[Ni(Me_4L)](ClO_4)_2$ for the $Ni^{III/II}$ couple (Fig. S5†). These observations indicate that the oxidation from Ni^{II} to Ni^{III}

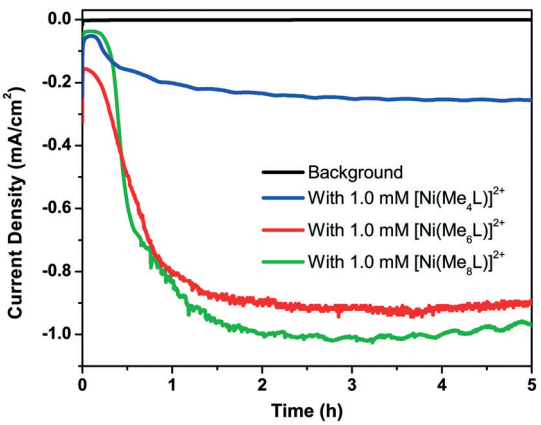

Fig. 4 Current density traces obtained in the CPE experiments with 1.0 mM $[Ni(Me_4L)](ClO_4)_2$ (blue), $[Ni(Me_6L)](ClO_4)_2$ (red) and $[Ni(Me_8L)](ClO_4)_2$ (green) at ITO electrodes (1.5 cm^2) in 0.10 M NaPi (pH 7.0) at 1.55 V *vs.* NHE without stirring. The background (black) is shown for comparison.

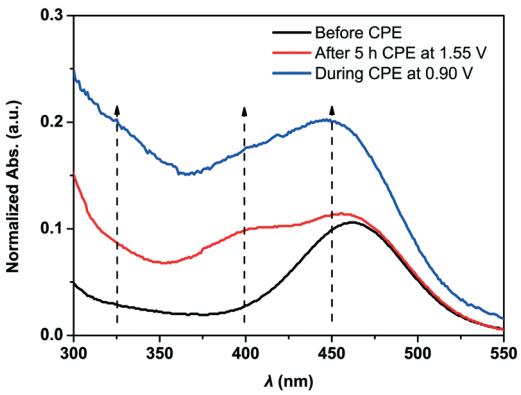

Fig. 5 The UV-vis spectra of 1.0 mM $[Ni(Me_6L)](ClO_4)_2$ in a 0.10 M NaPi buffer (pH 7.0) before (black) and after (red) 5 h of CPE at 1.55 V, and after 1 h of CPE at 0.90 V (blue).

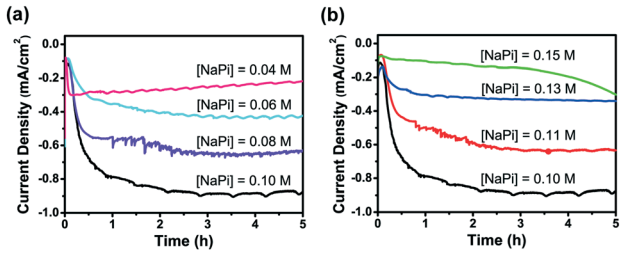

Fig. 6 Current density traces obtained in the CPE experiments with 1.0 mM $[Ni(Me_6L)](ClO_4)_2$ at ITO electrodes (1.5 cm^2) in NaPi buffer (pH 7.0) at 1.55 V with varying [NaPi]. (a) [NaPi] = 0.04–0.10 M; (b) [NaPi] = 0.10–0.15 M.

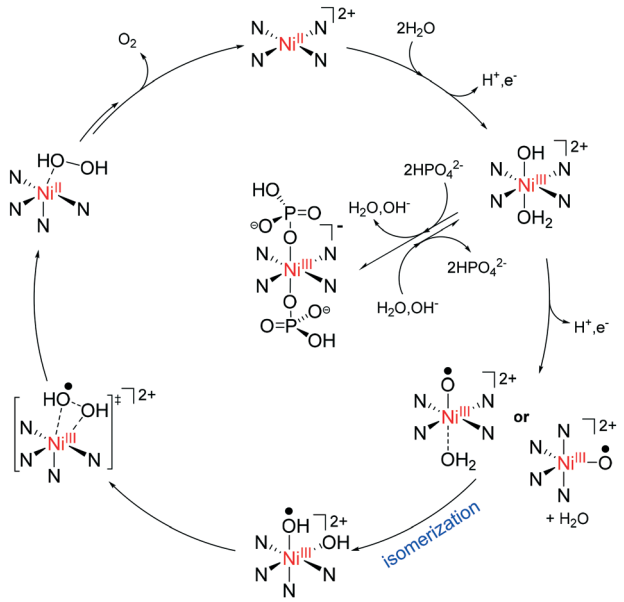

Fig. 7 The proposed mechanism for water oxidation by $[Ni^{II}(Me_xL)](ClO_4)_2$ (x = 4, 6 or 8) *via* intramolecular HO–OH coupling in a neutral NaPi system.

becomes more difficult with increasing methyl groups in these nickel complexes. In contrast, the potentials of their second oxidation waves show no significant change with varying number of methyl groups (Table 1).

To clarify the relationship between the methyl groups and the redox potentials, DFT calculations have been employed to shed light on the mystery. Based on the above observations in cyclic voltammetry, the two oxidation events of each nickel complex can be described as two steps of PCETs, as shown in Scheme 1. During the first PCET process, the d^8 Ni^{II} center is oxidized to a d^7 Ni^{III} center, with the deprotonation of one aqua ligand to a hydroxyl group. Then, the second PCET involves the oxidation of the Ni^{III}–hydroxyl species to formal Ni^{IV} species, possibly a Ni^{III}–(O$^{\bullet}$) radical species, two isomers of Ni^{IV}–$(OH)_2$ species or two isomers of Ni^{III}–(OH)(OH$^{\bullet}$) radical species. It can be considered that the first PCET consists of two concerted processes, the oxidation of Ni(II) to Ni(III) and the coordination of aqua/hydroxyl ligands to Ni(III), both of which will contribute to the change in free energy of the whole PCET. Inspired by the work of Busch *et al.*,[28] we speculate that, in the first PCET of $[Ni(Me_6L)]^{2+}$ and $[Ni(Me_8L)]^{2+}$, the coordination process will be substantially interfered by the steric effect of the axially oriented methyl groups (see Scheme 2). Meanwhile, the steric effect would be readily lowered when the bulky methyl groups are replaced by hydrogen atoms in $[Ni(Me_4L)](ClO_4)_2$.[29] Thus the $Ni^{III/II}$ oxidation of $[Ni(Me_4L)](ClO_4)_2$ occurs more easily. The steric effect could also be observed in the optimized structures of $[Ni^{III}(Me_xL)(OH)(H_2O)]^{2+}$ (x = 4, 6 and 8), where the distortion of the axial hydroxyl ligand increased with more methyl groups, as the O–Ni–N_1 and O–Ni–N_2 angles become larger along with increased methyl groups (Table 1 and Scheme 2). Therefore, it can be considered that the coordination process is limited by the axially oriented methyl groups (R_1 and R_2, see Scheme 2) in $[Ni(Me_6L)]^{2+}$ and $[Ni(Me_8L)]^{2+}$, leading to a net increase of the free energy and higher $Ni^{III/II}$ oxidation potentials. In contrast, the second PCET illustrated in Scheme 1 is not accompanied by a coordination process, which can circumvent the steric effect of the methyl groups. Consequently, the second oxidation would occur at almost the same redox potentials (Table 1). It should be mentioned that the Ni^{III}–O$^{\bullet}$ radical species is more likely to be the two-electron oxidized species compared with the Ni^{IV}=O oxo species due to the disfavored π back-bonding to the d^6 Ni^{IV} center (Fig. S6†).[9a,30] In addition, the $Ni^{IV}(OH)_2$ species or the Ni^{III}–(OH)(OH$^{\bullet}$) radical species are less possible to serve as the viable intermediates, as their calculated redox potentials are not consistent with the experimental values (Table S1†). Particularly, in our previous study on $[Ni(Me_6L)](ClO_4)_2$,[9a] it has been found that catalytic mechanisms with Ni^{IV}–$(OH)_2$ intermediates would induce much higher activation free energy barriers than the one with the Ni^{III}–O$^{\bullet}$ radical species. Finally, the DFT-calculated redox potentials of these two PCEs are in agreement with the measured values (Table 1), strongly supporting the proposed scheme.

Controlled potential electrolysis (CPE)

With a better understanding of the PCETs, the catalytic performances of $[Ni(Me_8L)]^{2+}$ and $[Ni(Me_4L)]^{2+}$ were evaluated by

Table 3 The calculated values of activation free energy ($\Delta G^{\neq}$) at the O–O formation step and free energy to achieve the phosphate coordination reaction

Complexes	$[Ni(Me_4L)](ClO_4)_2$	$[Ni(Me_6L)](ClO_4)_2$	$[Ni(Me_8L)](ClO_4)_2$
$\Delta G^{\neq}$ for O–O formation (kcal mol^{-1})	23.9	28.9	24.7
ΔG for phosphate coordination reaction (kcal mol^{-1})	−4.2	−1.4	+5.4

CPE at 1.55 V *vs.* NHE (~750 mV overpotential) in a three-compartment, gas-tight cell. The O_2 formation in the headspace was analyzed by gas chromatography. The results are summarized in Table 2. As shown in Fig. 4, the background current is negligible, while the catalytic current in the presence of 1.0 mM $[Ni(Me_8L)]^{2+}$ steadily increased within the initial 1 h, and then kept relatively stable to approximately 1.05 ± 0.05 mA cm^{-2} upon further electrolysis, which is higher than that of the reported $[Ni(Me_6L)]^{2+}$ (0.90 ± 0.03 mA cm^{-2}).[9a] Impressively, the current density value of 1.05 ± 0.05 mA cm^{-2} during the CPE with $[Ni(Me_8L)]^{2+}$ at a moderate overpotential (600–900 mV)[11a] is the highest one among the reported molecular WOCs based on nickel(II) complexes.[8] During 5 h of CPE with 1.0 mM $[Ni(Me_8L)]^{2+}$, 22.6 C of charge accumulated and 53.4 μmol of oxygen was detected, giving a Faradaic efficiency of 93% ± 5% and a turnover number (TON) of 15.2 ± 0.8 based on the catalyst molecules in the bulk solution (Fig. S7†). After pH adjustment of the used electrolyte back to 7.0, the current trace could be recovered in the second run (Fig. S8†), demonstrating the high stability of $[Ni(Me_8L)]^{2+}$ as a WOC. As for $[Ni(Me_4L)]^{2+}$, the current density was maintained at approximately 0.25 ± 0.02 mA cm^{-2} after an induction period (Fig. 4), with a Faradaic efficiency of 94% ± 5% and a TON value of 3.6 ± 0.3 (Fig. S9†). These values are much lower than those of $[Ni(Me_8L)]^{2+}$ and $[Ni(Me_6L)]^{2+}$ (Table 2), indicating the catalytic efficiency of $[Ni(Me_4L)]^{2+}$ is much lower than that of $[Ni(Me_8L)]^{2+}$ and $[Ni(Me_6L)]^{2+}$.

These macrocyclic nickel(II) complexes were found to be stable during CPE. For $[Ni(Me_8L)](ClO_4)_2$ and $[Ni(Me_4L)](ClO_4)_2$, all their CVs before and after long-term CPE experiments were almost identical (Fig. S10†), indicating no activity loss during water oxidation catalysis. Moreover, these WOCs were nearly quantitatively recrystallized from the electrolyte after CPE, as determined by the single-crystal X-ray diffraction (Fig. S11 and S12†) and PXRD (Fig. S13†), clearly demonstrating the intact nature of these nickel(II) complexes after CPE. Interestingly, we observed that the UV-vis spectra measured immediately after catalysis changed for both $[Ni(Me_8L)](ClO_4)_2$ and $[Ni(Me_4L)](ClO_4)_2$ (Fig. S14†), indicating new species could remain in the electrolyte after catalysis, and this will be further discussed later.

Evidence for homogeneous electrocatalysis

Even though the initial increase of current during CPE may have been considered as a sign of electrodeposition,[31] no heterogeneous catalysis was found during the CPE with $[Ni(Me_8L)](ClO_4)_2$ and $[Ni(Me_4L)](ClO_4)_2$ in a neutral NaPi system, as demonstrated by the following tests. Initially, repeated scans with $[Ni(Me_8L)](ClO_4)_2$ or $[Ni(Me_4L)](ClO_4)_2$ at a GC electrode were conducted (Fig. S1 and S3†). The CVs did not show increasing catalytic currents on repeated scanning, indicating the homogeneous nature of $[Ni(Me_8L)](ClO_4)_2$ and $[Ni(Me_4L)](ClO_4)_2$ in catalysis.[9a,32] Subsequently, the used GC electrode was rinsed with water after the above scans but not polished, and then cycled in a buffer-only solution. As shown in Fig. S15,† no catalytic current was observed compared to a polished electrode, further confirming that $[Ni(Me_8L)](ClO_4)_2$ and $[Ni(Me_4L)](ClO_4)_2$ are homogeneous WOCs. Additionally, adding 20% bipyridine in the solution with 1.0 mM $[Ni(Me_8L)](ClO_4)_2$ or $[Ni(Me_4L)](ClO_4)_2$ did not cause a current decrease, demonstrating the catalytic water oxidation is due to the complex rather than the free nickel ions (Fig. S16†).[33] After 5 h of CPE with $[Ni(Me_8L)](ClO_4)_2$, the used ITO electrode was gently rinsed with water, followed by cyclic voltammetry in a catalyst-free solution; no catalytic current was observed (Fig. S17a†). This observation demonstrates that no active heterogeneous WOC was deposited on the ITO electrode during the CPE with $[Ni(Me_8L)](ClO_4)_2$. The same conclusion can also be drawn in the case of $[Ni(Me_4L)](ClO_4)_2$ (Fig. S17b†). More importantly, the results of SEM and EDX further indicate that no Ni-based film or particle was deposited on the ITO surface after CPE with $[Ni(Me_8L)](ClO_4)_2$ or $[Ni(Me_4L)](ClO_4)_2$ (Fig. S18†). In summary, the above results clearly demonstrate that the nature of water oxidation catalysis by $[Ni(Me_8L)](ClO_4)_2$ or $[Ni(Me_4L)](ClO_4)_2$ is homogeneous.

The roles of phosphate anion

As noted before, two unique phenomena have been observed during the water oxidation catalyzed by these nickel complexes. One is that the UV-vis spectra of the electrolytes after CPE are different from the ones before CPE (Fig. S14†). The other one is that the catalytic current increases slowly to reach a plateau during CPE (Fig. 4). To unfold the above mystery, UV-vis spectroelectrochemistry (UV-SEC) of $[Ni(Me_6L)](ClO_4)_2$ was conducted, where CPE at 0.90 V was conducted in a UV-SEC cell containing 1.0 mM $[Ni(Me_6L)](ClO_4)_2$ in a 0.10 M NaPi buffer at pH 7.0. The applied oxidation potential of 0.90 V was supposed to achieve the oxidation of $[Ni^{II}(Me_6L)](ClO_4)_2$ to its Ni^{III} state (Fig. 2). As shown in Fig. 5 and Fig. S19,† a UV-vis spectrum was collected after 1 h of CPE at 0.90 V, which is similar to the one after 5 h of CPE at 1.55 V, and this spectrum required about 2 h to convert back into the original one (Fig. S19b†). These observations indicate that the newly formed species in the electrolyte after the CPE at 1.55 V is most likely to be a long-lived Ni^{III} species. Meyerstein *et al.* have found that $[Ni^{II}(Me_6L)](ClO_4)_2$ can be electrochemically oxidized to a Ni^{III}–hydroxyl species, $[Ni^{III}(Me_6L)(H_2O)(OH)]^{2+}$, followed by the replacement of axially coordinated H_2O and OH^- with two phosphate anions to generate the Ni^{III}–phosphate species, $[Ni^{III}(Me_6L)(HPO_4)_2]^-$, at pH 7.0.[34] As the axial coordination of HPO_4^{2-} anions can readily stabilize the Ni^{III} metal center, the Ni^{III}–phosphate species is much more long-lived than the Ni^{III}–hydroxyl species. Thus $[Ni^{III}(Me_6L)(HPO_4)_2]^-$ would remain in solution after CPE, causing different UV-vis spectra of the electrolytes. Indeed, the UV-vis spectra of the electrolytes after CPE could be slowly converted back into the initial ones after long-time standing (Fig. S19b†). Consequently, it is reasonable to assign $[Ni^{III}(Me_6L)(HPO_4)_2]^-$ as the newly formed species that

remained in the electrolyte after 5 h of CPE at 1.55 V. Similar phenomena can also be observed in the cases of $[Ni(Me_4L)](ClO_4)_2$ and $[Ni(Me_8L)](ClO_4)_2$ (Fig. S20 and S21†).

In contrast to the catalytically active Ni^{III}–hydroxyl species of $[Ni^{III}(Me_6L)(H_2O)(OH)]^{2+}$, the Ni^{III}–phosphate species of $[Ni^{III}(Me_6L)(HPO_4)_2]^-$ should be inactive as the axial positions are occupied by two HPO_4^{2-} anions. At the beginning of CPE, $[Ni^{II}(Me_6L)]^{2+}$ undergoes a 1 e^-/1 H^+ PCET process to generate the catalytically active species of $[Ni^{III}(Me_6L)(H_2O)(OH)]^{2+}$ [eqn (1)], which is quickly transformed to the catalytically inactive $[Ni^{III}(Me_6L)(HPO_4)_2]^-$ as a dominant species,[34] as described in eqn (2). According to eqn (2), the above two species would co-exist in the quasi-stagnant double layer between the anode and the electrolyte. At first, the catalytic current is low as only few active Ni^{III}–hydroxyl species remain. With increasing time of CPE, the concentrations of both $[Ni^{III}(Me_6L)(H_2O)(OH)]^{2+}$ and $[Ni^{III}(Me_6L)(HPO_4)_2]^-$ species would gradually increase, and an equilibrium can be reached after about 1 h of CPE in 0.1 M NaPi electrolyte. Therefore, the catalytic current would also slowly increase and finally reach a plateau after 1 h of CPE.

To identify the role of the phosphate anion during the catalytic water oxidation, CPE experiments at 1.55 V with $[Ni(Me_6L)](ClO_4)_2$ at varying concentrations of NaPi buffer (pH 7.0) were conducted. It is interesting to note that the catalytic currents firstly increased along with increasing concentrations of [NaPi] from 0.04 to 0.10 M (Fig. 6a), reaching a maximum current of 0.9 mA cm^{-2} at 0.10 M, and then decreased with further increasing concentrations of [NaPi] (Fig. 6b). This can be attributed to the double roles of [NaPi], being a proton acceptor and a coordination ligand. At lower concentrations of 0.04 to 0.10 M, [NaPi] mainly acts as a proton acceptor, thus the catalytic currents increase along with increasing concentrations of [NaPi]. However, further increasing the concentrations of [NaPi] would be favorable to the formation of inactive Ni^{III}–phosphate species, resulting in the decrease of the catalytic currents. For $[Ni(Me_8L)](ClO_4)_2$, the maximum catalytic current (1.0 mA cm^{-2}) during CPE also appears at a [NaPi] concentration of 0.10 M (Fig. S22†). It should be mentioned that it only took about half an hour of CPE for the catalytic current of $[Ni(Me_4L)](ClO_4)_2$ to reach a plateau, with the maximum catalytic current of 0.34 mA cm^{-2} appearing at a [NaPi] concentration of 0.08 M (Fig. S23†). This can be attributed to the lack of steric effects on the axial position of the Ni^{III} center, which results in fast and favorable axial coordination of phosphate anions with Ni^{III}.

$$\left[Ni^{II}(Me_6L)\right]^{2+} + 2H_2O \xrightarrow{-e^-,-H^+} \left[Ni^{III}(Me_6L)(H_2O)(OH)\right]^{2+} \quad (1)$$

$$\left[Ni^{III}(Me_6L)(H_2O)(OH)\right]^{2+} + 2HPO_4^{2-} \underset{}{\overset{k_{eq}}{\rightleftharpoons}} \left[Ni^{III}(Me_6L)(HPO_4)_2\right]^- + H_2O + OH^- \quad (2)$$

Mechanistic studies

As determined by CPE experiments (Fig. 4), the catalytic currents increase along with increasing methyl groups in the structures of the nickel complexes. Initially, we assumed that the different catalytic performances might be relevant to the activation energy at the rate-determining step, the O–O bond formation,[10b,35] in the water oxidation reaction. Thus, DFT calculations were carried out to further verify the catalytic mechanism and estimate the activation energy. As described in Fig. 7 and S24,† the most feasible O–O bond formation pathway is found to be the intramolecular HO–OH coupling from the *cis*-isomer intermediates, as we have discovered previously.[9a] Indeed, the peroxide intermediate can be detected in the electrolyte from continuous scanning for 100 cycles of cyclic voltammetry within the 0.5–1.6 V range or from a CPE experiment at 1.55 V with **1** as the example, using horseradish peroxidase and Ampliflu red as indicators (Fig. S25†). In contrast, other mechanisms, such as the water attack mechanism and water insertion mechanism, have been verified to be much less feasible (see Fig. S26–S29 in the ESI† for details). As shown in Table 3, the activation free energy at the O–O bond formation step of $[Ni(Me_6L)](ClO_4)_2$ ($\Delta G^{\neq}$ = 28.9 kcal mol^{-1}) is higher than that of $[Ni(Me_8L)](ClO_4)_2$ ($\Delta G^{\neq}$ = 24.7 kcal mol^{-1}), consistent with the observed lower catalytic activity of $[Ni(Me_6L)](ClO_4)_2$. However, the activation free energy of $[Ni(Me_4L)](ClO_4)_2$ ($\Delta G^{\neq}$ = 23.9 kcal mol^{-1}) was found to be the lowest one among the three complexes, inconsistent with its catalytic activity being the lowest among the three catalysts. Therefore, the different catalytic performances should also be affected by other factors.

As demonstrated before, the axial coordination of phosphate anions to the Ni^{III} centers will decrease the initial catalytic current during CPE, and such axial coordination is likely to be sterically hindered by the axially oriented methyl groups (see Scheme 2). That is, the phosphate coordination reaction acts as a side reaction that limits the catalytic rate. Consequently, it is reasonable to speculate that the larger steric effect from the axially oriented methyl groups can result in higher catalytic currents by suppressing the phosphate coordination reactions. This speculation is readily supported by the calculations on the phosphate coordination reactions with the three nickel complexes. As shown in Table 3, the phosphate coordination reaction with $[Ni(Me_4L)](ClO_4)_2$ required the most negative free energy (ΔG = −4.2 kcal mol^{-1}). In comparison, the free energy to achieve the coordination reaction with $[Ni(Me_6L)](ClO_4)_2$ was determined to be more positive (ΔG = −1.4 kcal mol^{-1}) and the one with $[Ni(Me_8L)](ClO_4)_2$ was the highest (ΔG = +5.4 kcal mol^{-1}). It should be noted that, other coordination modes, such as monophosphate coordination or bidentate phosphate coordination, are less thermodynamically favored on the basis of calculation (Fig. S30†). Thus, despite some deviations in the calculation, the order of the free energy was qualitatively in line with both the observed orders of the steric effect (the amount of axially oriented methyl groups) and the catalytic

activity (Fig. 4). Based on the above results, it can be considered that the higher steric effect may disfavor the phosphate coordination reaction and thus enhance the catalytic activity.

Conclusions

In summary, three tetraazamacrocyclic nickel(II) complexes with varying numbers of methyl groups have been utilized as homogeneous electrocatalysts for water oxidation. These WOCs exhibit high catalytic currents, Faradaic efficiencies and stability in a mild, neutral aqueous system. Most importantly, several lines of evidence suggest that the steric effect from the axially oriented methyl groups plays a key role in their different catalytic performances, in which the steric effect on the axial position of the oxidized Ni^{III} center can suppress the formation of inactive Ni^{III}–phosphate species to result in better catalytic performance. Such a steric effect in catalytic water oxidation has not been documented so far. Based on the aforementioned results, a reasonable mechanism was given for these homogeneous nickel WOCs. The present work opens a new avenue for optimizing the catalytic performance of homogeneous WOCs.

Conflicts of interest

There are no conflicts of interest to declare.

Acknowledgements

This work was financially supported by the 973 Program of China (2014CB845602), NSFC (Grant No. 21331007 and 21121061), and NSF of Guangdong Province (S2012030006240).

Notes and references

1 (*a*) M. D. Kärkäs, T. Åkermark, H. Chen, J. Sun and B. Åkermark, *Angew. Chem., Int. Ed.*, 2013, **52**, 4274; (*b*) M. Zhang, Y. L. Huang, J. W. Wang and T. B. Lu, *J. Mater. Chem. A*, 2016, **4**, 1819–1827; (*c*) Y.-N. Gong, T. Ouyang, C.-T. He and T.-B. Lu, *Chem. Sci.*, 2016, **7**, 1070–1075.

2 F. Zhang, Y. Shi, T. Xue, J. Zhang, Y. Liang and B. Zhang, *Sci. China Mater.*, 2017, **60**, 324–334.

3 S. M. Barnett, K. I. Goldberg and J. M. Mayer, *Nat. Chem.*, 2012, **4**, 498–502.

4 (*a*) J. J. Concepcion, J. W. Jurss, J. L. Templeton and T. J. Meyer, *J. Am. Chem. Soc.*, 2008, **130**, 16462–16463; (*b*) L. Duan, F. Bozoglian, S. Mandal, B. Stewart, T. Privalov, A. Llobet and L. Sun, *Nat. Chem.*, 2012, **4**, 418–423; (*c*) L. Tong and R. P. Thummel, *Chem. Sci.*, 2016, **7**, 6591–6603; (*d*) S. Roeser, F. Bozoglian, C. J. Richmond, A. B. League, M. Z. Ertem, L. Francàs, P. Miró, J. Benet-Buchholz, C. J. Cramer and A. Llobet, *Catal. Sci. Technol.*, 2016, **6**, 5088–5101; (*e*) M. Schulze, V. Kunz, P. D. Frischmann and F. Wurthner, *Nat. Chem.*, 2016, **8**, 576–583.

5 (*a*) J. F. Hull, D. Balcells, J. D. Blakemore, C. D. Incarvito, O. Eisenstein, G. W. Brudvig and R. H. Crabtree, *J. Am. Chem. Soc.*, 2009, **131**, 8730–8731; (*b*) J. M. Thomsen, S. W. Sheehan, S. M. Hashmi, J. Campos, U. Hintermair, R. H. Crabtree and G. W. Brudvig, *J. Am. Chem. Soc.*, 2014, **136**, 13826–13834.

6 (*a*) M. Domarus, M. L. Kuznetsov, J. Marcalo, A. J. Pombeiro and J. A. da Silva, *Angew. Chem., Int. Ed.*, 2016, **55**, 1489–1492; (*b*) M.-P. Santoni, G. La Ganga, V. Mollica Nardo, M. Natali, F. Puntoriero, F. Scandola and S. Campagna, *J. Am. Chem. Soc.*, 2014, **136**, 8189–8192.

7 (*a*) J. Limburg, J. S. Vrettos, L. M. Liable-Sands, A. L. Rheingold, R. H. Crabtree and G. W. Brudvig, *Science*, 1999, **283**, 1524–1527; (*b*) W. T. Lee, S. B. Munoz 3rd, D. A. Dickie and J. M. Smith, *Angew. Chem., Int. Ed.*, 2014, **53**, 9856–9859; (*c*) L. Ma, Q. Wang, W. L. Man, H. K. Kwong, C. C. Ko and T. C. Lau, *Angew. Chem., Int. Ed.*, 2015, **54**, 5246–5249.

8 (*a*) W. C. Ellis, N. D. McDaniel, S. Bernhard and T. J. Collins, *J. Am. Chem. Soc.*, 2010, **132**, 10990–10991; (*b*) J. L. Fillol, Z. Codola, I. Garcia-Bosch, L. Gomez, J. J. Pla and M. Costas, *Nat. Chem.*, 2011, **3**, 807–813; (*c*) M. Okamura, M. Kondo, R. Kuga, Y. Kurashige, T. Yanai, S. Hayami, V. K. Praneeth, M. Yoshida, K. Yoneda, S. Kawata and S. Masaoka, *Nature*, 2016, **530**, 465–468.

9 (*a*) M. Zhang, M. T. Zhang, C. Hou, Z. F. Ke and T. B. Lu, *Angew. Chem., Int. Ed.*, 2014, **53**, 13042–13048; (*b*) Y. Han, Y. Wu, W. Lai and R. Cao, *Inorg. Chem.*, 2015, **54**, 5604–5613; (*c*) G. Y. Luo, H. H. Huang, J. W. Wang and T. B. Lu, *ChemSusChem*, 2016, **9**, 485–491; (*d*) L. Wang, L. Duan, R. B. Ambre, Q. Daniel, H. Chen, J. Sun, B. Das, A. Thapper, J. Uhlig, P. Dinér and L. Sun, *J. Catal.*, 2016, **335**, 72–78; (*e*) X. B. Han, Y. G. Li, Z. M. Zhang, H. Q. Tan, Y. Lu and E. B. Wang, *J. Am. Chem. Soc.*, 2015, **137**, 5486–5493.

10 (*a*) Q. Yin, J. M. Tan, C. Besson, Y. V. Geletii, D. G. Musaev, A. E. Kuznetsov, Z. Luo, K. I. Hardcastle and C. L. Hill, *Science*, 2010, **328**, 342–345; (*b*) D. Wang and J. T. Groves, *Proc. Natl. Acad. Sci. U. S. A.*, 2013, **110**, 15579–15584; (*c*) B.-T. Chen, N. Morlanés, E. Adogla, K. Takanabe and V. O. Rodionov, *ACS Catal.*, 2016, **6**, 4647–4652.

11 (*a*) S. M. Barnett, K. I. Goldberg and J. M. Mayer, *Nat. Chem.*, 2012, **4**, 498–502; (*b*) P. Garrido-Barros, I. Funes-Ardoiz, S. Drouet, J. Benet-Buchholz, F. Maseras and A. Llobet, *J. Am. Chem. Soc.*, 2015, **137**, 6758–6761; (*c*) L. Yu, X. Du, Y. Ding, H. Chen and P. Zhou, *Chem. Commun.*, 2015, **51**, 17443–17446; (*d*) X. J. Su, M. Gao, L. Jiao, R. Z. Liao, P. E. Siegbahn, J. P. Cheng and M. T. Zhang, *Angew. Chem., Int. Ed.*, 2015, **54**, 4909–4914; (*e*) H. H. Huang, J. W. Wang, P. Sahoo, D. C. Zhong and T. B. Lu, *Chem. Commun.*, 2017, **53**, 9324–9327; (*f*) P. Garrido-Barros, C. Gimbert-Surinach, D. Moonshiram, A. Picon, P. Monge, V. S. Batista and A. Llobet, *J. Am. Chem. Soc.*, 2017, **139**, 12907–12910; (*g*) J. Wang, H. Huang and T. Lu, *Chin. J. Chem.*, 2017, **35**, 586–590.

12 (*a*) T. Nakazono, A. R. Parent and K. Sakai, *Chem. Commun.*, 2013, **49**, 6325–6327; (*b*) B. Zhang, F. Li, F. Yu, H. Cui, X. Zhou, H. Li, Y. Wang and L. Sun, *Chem. – Asian J.*, 2014, **9**, 1515–1518; (*c*) L. D. Wickramasinghe, R. Zhou, R. Zong, P. Vo, K. J. Gagnon and R. P. Thummel, *J. Am. Chem. Soc.*,

2015, **137**, 13260–13263; (*d*) T. Zhang, C. Wang, S. Liu, J. L. Wang and W. Lin, *J. Am. Chem. Soc.*, 2014, **136**, 273–281.
13 R. H. Crabtree, *Chem. Rev.*, 2015, **115**, 127–150.
14 L. Yu, Y. Ding, M. Zheng, H. Chen and J. Zhao, *Chem. Commun.*, 2016, **52**, 14494–14497.
15 J. Schneider, H. F. Jia, K. Kobiro, D. E. Cabelli, J. T. Muckerman and E. Fujita, *Energy Environ. Sci.*, 2012, **5**, 9502–9510.
16 (*a*) N. Kaveevivitchai, L. Kohler, R. Zong, M. El Ojaimi, N. Mehta and R. P. Thummel, *Inorg. Chem.*, 2013, **52**, 10615–10622; (*b*) J. L. Boyer, D. E. Polyansky, D. J. Szalda, R. Zong, R. P. Thummel and E. Fujita, *Angew. Chem., Int. Ed.*, 2011, **50**, 12600–12604.
17 L. G. Warner and D. H. Busch, *J. Am. Chem. Soc.*, 1969, **91**, 4092–4101.
18 L. Jiang, X. L. Feng and T. B. Lu, *Cryst. Growth Des.*, 2005, **5**, 1469–1475.
19 Y.-C. Lin, T. K. Misra, T.-H. Lu, M. S. Joseph and C.-S. Chung, *Eur. J. Inorg. Chem.*, 2006, **2006**, 994–1005.
20 R. W. Hay and B. Jeragh, *J. Chem. Soc., Dalton Trans.*, 1977, 1261–1266.
21 R. W. Hay and B. Jeragh, *J. Chem. Soc., Dalton Trans.*, 1982, 1531–1539.
22 J. Shen, M. Wang, P. Zhang, J. Jiang and L. Sun, *Chem. Commun.*, 2017, **53**, 4374–4377.
23 M. J. Frisch, G. W. Trucks, H. B. Schlegel, G. E. Scuseria, M. A. Robb, J. R. Cheeseman, G. Scalmani, V. Barone, G. A. Petersson, H. Nakatsuji, X. Li, M. Caricato, A. Marenich, J. Bloino, B. G. Janesko, R. Gomperts, B. Mennucci, H. P. Hratchian, J. V. Ortiz, A. F. Izmaylov, J. L. Sonnenberg, D. Williams-Young, F. Ding, F. Lipparini, F. Egidi, J. Goings, B. Peng, A. Petrone, T. Henderson, D. Ranasinghe, V. G. Zakrzewski, J. Gao, N. Rega, G. Zheng, W. Liang, M. Hada, M. Ehara, K. Toyota, R. Fukuda, J. Hasegawa, M. Ishida, T. Nakajima, Y. Honda, O. Kitao, H. Nakai, T. Vreven, K. Throssell, J. A. Montgomery, Jr., J. E. Peralta, F. Ogliaro, M. Bearpark, J. J. Heyd, E. Brothers, K. N. Kudin, V. N. Staroverov, T. Keith, R. Kobayashi, J. Normand, K. Raghavachari, A. Rendell, J. C. Burant, S. S. Iyengar, J. Tomasi, M. Cossi, J. M. Millam, M. Klene, C. Adamo, R. Cammi, J. W. Ochterski, R. L. Martin, K. Morokuma, O. Farkas, J. B. Foresman and D. J. Fox, *Gaussian 09, Revision A.02*, Gaussian, Inc., Wallingford, CT, 2016.
24 A. D. Becke, *J. Chem. Phys.*, 1993, **98**, 1372–1377.
25 M. Dolg, U. Wedig, H. Stoll and H. Preuss, *J. Chem. Phys.*, 1987, **86**, 866–872.
26 C. Y. Legault, *CYLview, 1.0b*, Université de Sherbrooke, 2009, http://www.cylview.org.
27 (*a*) W.-P. To, T. Wai-Shan Chow, C.-W. Tse, X. Guan, J.-S. Huang and C.-M. Che, *Chem. Sci.*, 2015, **6**, 5891–5903; (*b*) M. T. Zhang, Z. Chen, P. Kang and T. J. Meyer, *J. Am. Chem. Soc.*, 2013, **135**, 2048–2051.
28 F. V. Lovecchio, E. S. Gore and D. H. Busch, *J. Am. Chem. Soc.*, 1974, **96**, 3109–3118.
29 L. J. DeHayes and D. H. Busch, *Inorg. Chem.*, 1973, **12**, 1505–1513.
30 K. P. O'Halloran, C. Zhao, N. S. Ando, A. J. Schultz, T. F. Koetzle, P. M. Piccoli, B. Hedman, K. O. Hodgson, E. Bobyr, M. L. Kirk, S. Knottenbelt, E. C. Depperman, B. Stein, T. M. Anderson, R. Cao, Y. V. Geletii, K. I. Hardcastle, D. G. Musaev, W. A. Neiwert, X. Fang, K. Morokuma, S. Wu, P. Kogerler and C. L. Hill, *Inorg. Chem.*, 2012, **51**, 7025–7031.
31 (*a*) A. Singh, S. L. Y. Chang, R. K. Hocking, U. Bach and L. Spiccia, *Energy Environ. Sci.*, 2013, **6**, 579–586; (*b*) M. K. Coggins, M. T. Zhang, Z. Chen, N. Song and T. J. Meyer, *Angew. Chem., Int. Ed.*, 2014, **53**, 12226–12230; (*c*) M. A. Asraf, H. A. Younus, M. Yusubov and F. Verpoort, *Catal. Sci. Technol.*, 2015, **5**, 4901–4925.
32 A. Singh, S. L. Y. Chang, R. K. Hocking, U. Bach and L. Spiccia, *Catal. Sci. Technol.*, 2013, **3**, 1725–1732.
33 J.-W. Wang, P. Sahoo and T.-B. Lu, *ACS Catal.*, 2016, **6**, 5062–5068.
34 E. Zeigerson, I. Bar, J. Bernstein, L. J. Kirschenbaum and D. Meyerstein, *Inorg. Chem.*, 1982, **21**, 73–80.
35 (*a*) M. K. Coggins, M.-T. Zhang, A. K. Vannucci, C. J. Dares and T. J. Meyer, *J. Am. Chem. Soc.*, 2014, **136**, 5531–5534; (*b*) J. J. Concepcion, J. W. Jurss, M. K. Brennaman, P. G. Hoertz, A. O. Patrocinio, N. Y. Murakami Iha, J. L. Templeton and T. J. Meyer, *Acc. Chem. Res.*, 2009, **42**, 1954–1965; (*c*) J. W. Vickers, J. M. Sumliner, H. Lv, M. Morris, Y. V. Geletii and C. L. Hill, *Phys. Chem. Chem. Phys.*, 2014, **16**, 11942–11949; (*d*) Z. Chen, J. J. Concepcion, X. Hu, W. Yang, P. G. Hoertz and T. J. Meyer, *Proc. Natl. Acad. Sci. U. S. A.*, 2010, **107**, 7225–7229; (*e*) N. Song, J. J. Concepcion, R. A. Binstead, J. A. Rudd, A. K. Vannucci, C. J. Dares, M. K. Coggins and T. J. Meyer, *Proc. Natl. Acad. Sci. U. S. A.*, 2015, **112**, 4935–4940.